Journal of Applied Electrochemistry **33**: 373–379, 2003.

Effect of benzylideneacetone on the electrodeposition mechanism of Zn–Co alloy

G. TREJO[1], R. ORTEGA[1], Y. MEAS[1], E. CHAINET[2] and P. OZIL[2]
[1]*Centro de Investigación y Desarrollo Tecnológico en Electroquímica (CIDETEQ), Parque Tecnológico Sanfandila, Pedro Escobedo Querétaro AP 064, CP 76700, México*
[2]*Laboratoire d'Electrochimie et de Physico-Chimie des Matériaux et des interfaces (UMR INPG-CNRS 5631 associée à l'UJF), ENSEEG, BP 45, 38402 Saint Martin d'Hères, France*

Received 25 May 2002; accepted in revised form 19 December 2002

Key words: additives, benzylideneacetone, electrodeposition, zinc–cobalt alloys

Abstract

The influence of benzylideneacetone (BA) on the mechanism of Zn–Co alloy electrodeposition onto AISI 1018 steel was studied in chloride acidic solutions. Results indicate that BA modifies the exchange current densities of zinc and cobalt such that the alloy is electrodeposited via a normal codeposition mechanism. Analysis of the deposits by Auger spectroscopy and X-ray diffraction shows that BA increases the cobalt concentration in the electrodeposited alloys and gives deposits with a constant concentration profile of both Zn and Co. BA also inhibits the formation of zinc hydroxide in the initial deposition stages, which supports the proposed mechanism of normal codeposition. Finally, it is shown that BA modifies the morphology of the deposits by inducing a reduction in the cluster size, leading to compact, smooth and shiny coatings.

1. Introduction

Zn–Co alloys are widely used in industry as protective coatings on account of their excellent corrosion resistance, which is superior to that of traditional pure zinc coatings. The electrodeposition of Zn–Co alloys is generally classified as an anomalous codeposition process [1] due to the preferential deposition of the less noble metal (Zn). Several hypotheses have been proposed to explain this anomalous codeposition. The most accepted hypothesis explains the anomalous behaviour in terms of the precipitation and adsorption of a zinc hydroxide film at the electrode surface [2] that induces zinc reduction. This zinc hydroxide film is formed due to the increase in interfacial pH during the simultaneous electrochemical reaction of hydrogen evolution. An alternative hypothesis, proposed by Nicol et al. [3], suggests that the underpotential deposition (UPD) of Zn inhibits the deposition of Co. Recently, Yan et al. [4] developed the model of hydroxide oscillation, in which the anomalous codeposition of Zn–Co alloys results from the formation of alternating zinc hydroxide layers whose thickness changes periodically. Other authors [5–8] have attributed the anomalous codeposition to the fact that the exchange current densities of the iron group metals (Fe, Co, Ni) are generally lower than that of zinc, which favours the preferential deposition of zinc. Higashi et al. [2] showed that the transition from anomalous to normal codeposition occurs as a result of changes in the applied current density during the electrodeposition of zinc alloys in acidic medium. Similar results were obtained by Fratesi et al. [9], who studied the influence of current density, temperature and cobalt concentration in the bath on the composition and morphology of electrodeposited Zn–Co alloys. Yunus et al. [10] found that the codeposition mechanism depended on the Zn(II)/Co(II) concentration ratio in a sulfate medium, and Vallés et al. [11–15] observed similar behaviour in chloride based solutions.

In the present study, the effect of benzylideneacetone (BA) on the electrodeposition of Zn–Co alloy onto AISI 1018 steel is investigated. The focus of this work is the codeposition mechanism, with attention also being given to deposit morphology and composition. Voltammetry was used to study the codeposition mechanism, and techniques such as scanning electron microscopy (SEM), X-ray diffraction (XRD) and Auger electron spectroscopy were used to characterize the deposits obtained under different conditions.

2. Experimental details

Zn–Co deposits were obtained from a base solution of 0.1 M $ZnCl_2$ + 0.1 M $CoCl_2 \cdot 6H_2O$ in a 2.8 M KCl + 0.32 M H_3BO_3 electrolyte, at pH 5, with a range of BA concentrations (0.0, 0.01, 0.1, 0.2, 0.4 g L^{-1}). All chemicals were of analytic grade and solutions were prepared using deionized water (18 MΩ cm^{-1}).

The electrochemical study was performed in a conventional three-electrode cell with a water jacket. The working electrode was a disc of AISI 1018 steel of geometrical area 0.07 cm^2 enclosed in Teflon. A saturated calomel electrode (SCE) was the reference electrode and a graphite bar the counter electrode. Prior to each experiment, the working electrode was polished to a mirror finish with 0.05 μm alumina (Buehler). Before each series of experiments, the solutions were bubbled with ultra-pure nitrogen (Linde) for 15 min and a nitrogen atmosphere was maintained during the experiments. The temperature was controlled at 25 °C using a Cole Parmer water circulation system.

The electrochemical experiments were carried out using a potentiostat/galvanostat (EG&G PAR model 273A) coupled to a personal computer equipped with EG&G M270 data acquisition software.

The characterization of the coatings was performed on deposits grown potentiostatically from solutions with a range of BA concentrations, using discs of 1018 steel of area 1 cm^2 as substrate. The coating thickness (6.0 μm) was measured by X-ray fluorescence (Fischer System XUVM).

Coating morphology was evaluated using a scanning electron microscope (Jeol model DSM-5400LV) coupled to an energy dispersion spectrometer (EDS) analyser (Kevex). The topography of the coatings was analysed by a profilometer (Handysurf model E-35A). The identification of the deposited phases was carried out by X-ray diffraction (XRD) using a Phillips diffractometer. The profile of the relative concentration of the elements was obtained using a scanning Auger microprobe (Physical Electronics model PHI 660), sputtering the sample with Ar^+ ions accelerated to 3 keV. The sputtering rate was 5 nm min^{-1}.

3. Results and discussion

3.1. *Cyclic voltammetry study*

To evaluate the electrochemical behaviour of zinc and cobalt individually, a preliminary study was carried out by cyclic voltammetry. In these experiments, solutions containing 0.1 M $ZnCl_2$ or 0.1 M $CoCl_2 \cdot 6H_2O$ in 2.8 M KCl + 0.32 M H_3BO_3 with a range of BA concentrations were used.

The preliminary experiments showed that BA has no electrochemical activity under the experimental conditions used in this study. Figure 1 shows typical voltammograms obtained from zinc solutions with and without BA. During the cathodic potential scan only a reduction peak (C_{Zn}) is observed; the peak potential ($E_{C,Zn}$) shifts to more negative values as the BA concentration in the solution is increased. When the potential scan is reversed, an anodic peak (A_{Zn}) appears at −1.05 V vs SCE ($E_{A,Zn}$). As the BA concentration is increased, the current density of the peak A_{Zn} decreases and the peak shifts to more positive potentials.

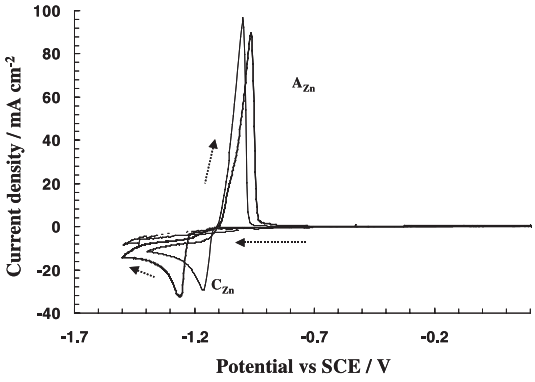

Fig. 1. Typical voltammograms obtained on 1018 steel from 0.1 M $ZnCl_2$ in 2.8 M KCl + 0.32 M H_3BO_3, pH 5.0, at different concentrations of BA: (——) 0.0 g L^{-1}, (——) 0.2 g L^{-1}. $v = 30$ mV s^{-1}. The supporting electrolyte 2.8 M KCl + 0.32 M H_3BO_3 + 0.2 g L^{-1} BA is also shown.

Figure 2 shows the effect of BA on the electrochemical response of cobalt. In the absence of BA, two reduction processes are observed: cobalt reduction (peak C_{Co}) and hydrogen evolution. In the anodic scan, a shoulder prior to cobalt oxidation (peak A_{Co}) is observed, which is attributed to the oxidation of the hydrogen formed during the cathodic scan. In the presence of BA, the oxidation (A_{Co}) and reduction (C_{Co}) peaks are slightly shifted toward more negative and positive potentials, respectively, when the BA concentration is increased. Furthermore, the current densities of the two peaks increase with increasing BA concentration.

The electrochemical behaviour of the Zn–Co alloys was studied from a base solution with a range of BA concentrations. The potential scan was started in the cathodic direction from the rest potential in the potential range 0.2 to −1.65 V vs SCE. Figure 3 shows typical voltammograms obtained from solutions with and without BA.

In the absence of BA, three reduction processes (Ic, IIc and IIIc) are clearly observed. When the scan is reversed, three oxidation peaks (Ia, IIa and IIIa) are

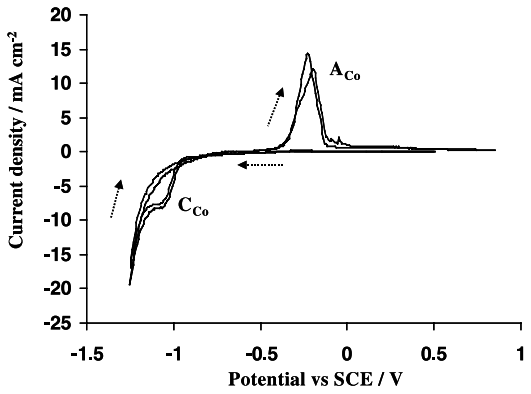

Fig. 2. Typical voltammograms obtained on 1018 steel from 0.1 M $CoCl_2 \cdot 6H_2O$ in 2.8 M KCl + 0.32 M H_3BO_3, at different concentrations of BA: (——) 0.0 g L^{-1}, (——) 0.2 g L^{-1}. $v = 30$ mV s^{-1}.

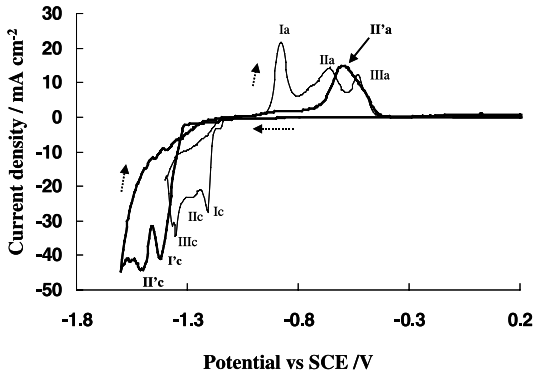

Fig. 3. Typical voltammograms obtained on 1018 steel from 0.1 M $ZnCl_2$ + 0.1 M $CoCl_2 \cdot 6H_2O$ in 2.8 M KCl + 0.32 M H_3BO_3, pH 5.0, at different concentrations of BA: (——) 0.0 g L^{-1}, (——) 0.2 g L^{-1}. $v = 30$ mV s^{-1}.

observed in the potential range −0.95 to −0.40 V vs SCE. As suggested by Jovic et al. [16], the detection of multiple peaks during the electrochemical oxidation of alloys can be attributed to the dissolution of the metals in the alloy via different intermediate phases. Thus, the voltammetric response gives information regarding the characteristics of the components of the alloy and the structure of the deposited phases.

The observed oxidation peaks were between the oxidation potentials of pure zinc (−1.05 V vs SCE) and pure cobalt (−0.19 V vs SCE), supporting the assignment of these peaks to the oxidation of Zn–Co compounds. Similar results have been reported by Vallés et al. [11–15, 17], who proposed the sequential oxidation of different alloy phases. In order to identify these phases, Zn–Co deposits were obtained at −1.35 V vs SCE and oxidized in different potential ranges (as explained below). The obtained solutions were analysed by inductively coupled plasma spectrophotometry (ICP) to evaluate the chemical composition of the dissolved deposits. The deposits obtained were dissolved in three consecutive oxidation stages, according to the observed peak potentials [−1.09 to −0.85 V vs SCE (peak Ia), −0.85 to −0.6 V vs SCE (peak IIa) and −0.6 to −0.4 V vs SCE (peak IIIa)]. The chemical compositions of the products associated with each peak were as follows: peak Ia, 98.9% Zn, 1.0% Co; peak IIa: 98.2% Zn, 1.7% Co; and peak IIIa: 34.0% Zn, 65.9% Co. These results show that peaks Ia and IIa are associated with the oxidation of a Zn-rich matrix and peak IIIa corresponds to oxidation of a Co-rich matrix.

Introduction of BA causes an important change in the voltammograms. During the cathodic scan, two reduction peaks (I′c, II′c) are observed at more cathodic potentials than those observed in the absence of BA. This shift can be attributed to the effect of the adsorption of BA, which induces an overpotential in the alloy deposition process [18, 19]. During the anodic potential scan, a small anodic current density is observed in the range −0.95 to −0.65 V vs SCE, and only one peak appears at more anodic potentials in the range −0.65 to −0.45 V vs SCE (peak II′a). Zn–Co deposits were obtained at −1.55 V vs SCE and oxidized in both potential ranges. The chemical compositions of the products associated with these signals were evaluated as 71.2% Zn, 28.7% Co and 61.4% Zn, 38.4% Co, respectively.

3.2. *Switching potentials (E_λ)*

To identify the oxidation peaks, the voltammetry with switching potential technique was employed. The potential scan was started in the cathodic direction from the rest potential and was inverted at different potential values (switching potential, E_λ). E_λ values were chosen to be within the zone where the reduction processes are observed in the voltammograms. Figure 4 shows the voltammograms obtained from a solution without BA at different switching potentials (E_λ). When $E_{\lambda 4} = -1.40$ V vs SCE, three anodic peaks (Ia, IIa and IIIa) are observed, corresponding to the oxidation of Zn–Co alloy [12]. When $E_{\lambda 3} = -1.27$ V vs SCE, in the potential region of peak IIc, a decrease in the current density of peaks Ia, IIa and IIIa is observed. In addition, a new peak, A_{Zn}, is observed at a potential of about −1.0 V vs SCE. This peak is associated with the oxidation of pure Zn [20]. At more anodic values of E_λ, for example, $E_{\lambda 1}$, only the peak A_{Zn} is observed. Therefore, when $E_\lambda > -1.27$ V vs SCE zinc metal is preferentially deposited with respect to cobalt, as would be expected for a process involving anomalous codeposition of Zn–Co alloy [2, 11–13].

A similar study was carried out on solutions containing BA. The results obtained at different values of E_λ in the range −1.55 to −1.3 V vs SCE are shown in Figure 5. When E_λ is −1.55 V vs SCE ($E_{\lambda 3}$), only the oxidation of the Zn–Co alloy is observed. At more anodic switching potentials ($E_{\lambda 2} = -1.4$ V vs SCE), two anodic peaks are observed which correspond to the oxidation of different phases of the Zn–Co alloy. When the potential was switched at more anodic potentials ($E_{\lambda 1} = -1.33$ V vs SCE), no deposit formation was observed.

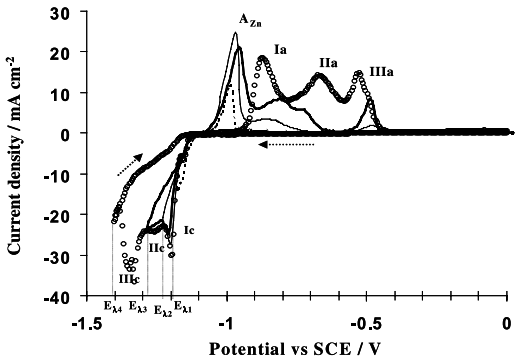

Fig. 4. Voltammograms obtained on 1018 steel from 0.1 M $ZnCl_2$ + 0.1 M $CoCl_2 \cdot 6H_2O$ in 2.8 M KCl + 0.32 M H_3BO_3, pH 5.0, in the absence of BA at different values of E_λ: $E_{\lambda 1}$ (- - - -) = −1.18, $E_{\lambda 2}$ (——) = −1.22, $E_{\lambda 3}$ (——) = −1.27, $E_{\lambda 4}$ (○○○) = −1.4 V vs SCE.

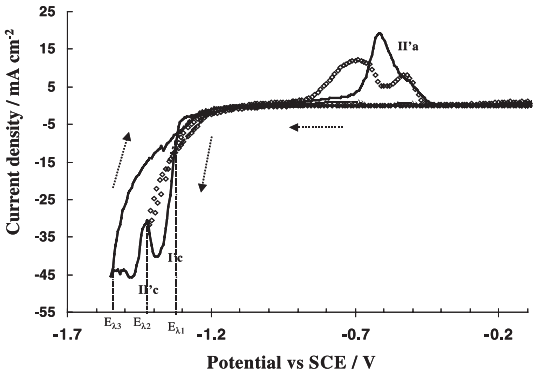

Fig. 5. Voltammograms obtained on 1018 steel from 0.1 M $ZnCl_2$ + 0.1 M $CoCl_2.6\,H_2O$ in 2.8 M KCl + 0.32 M H_3BO_3, pH 5.0, with 0.2 g L^{-1} of BA at different values of E_λ: $E_{\lambda 1}$ (—) = −1.33, $E_{\lambda 2}$ (◇◇◇) = −1.4, $E_{\lambda 3}$ (——) = −1.55 V vs SCE.

An important feature of the results presented above is that the oxidation of pure zinc is not observed in the range of E_λ studied. On the basis of this observation, it is proposed that BA inhibits the preferential deposition of zinc and favours the normal codeposition of the Zn–Co alloy.

3.3. *Voltammetric study using a rotating disc electrode (RDE)*

A RDE voltammetric study ($v = 3$ mV s^{-1}, $\omega =$ 2500 rpm) was carried out to determine the influence of BA on the exchange current density (i_0) of both zinc and cobalt in the presence of the following concentrations of BA: 0.0, 0.02, 0.1, 0.2 and 0.4 g L^{-1}. Prior to each experiment, a layer of the studied metal was electrodeposited on the steel electrode.

Figure 6(a) shows the polarization curves for the reduction of Zn in the presence of different concentrations of BA. The zinc reduction curves undergo a cathodic shift as the BA concentration in the solution is increased, indicating that BA induces an overpotential for the electrodeposition of zinc.

Figure 6(b) shows the polarization curves obtained during the reduction of cobalt in the presence of different concentrations of BA. An increase in the limit current density ($i_{\mathrm{lim,Co}}$) with increasing BA concentration is observed. The maximum value of $i_{\mathrm{lim,Co}}$ occurs at a BA concentration of 0.2 g L^{-1}. Furthermore, a small anodic shift is observed in the overpotential for the reduction of cobalt in the presence of BA.

Thus, the action of BA in Zn electrodeposition differs from that in Co electrodeposition: BA retards the discharge process of zinc, whereas it increases the current density of cobalt, facilitating the deposition of this metal. This behaviour favours the normal codeposition of the Zn–Co alloy. The mechanism by which BA acts in these systems is complex and has been little studied. Mockute et al. [18] have shown that during the electrolysis process BA decomposes into diverse compounds including benzaldehyde (BZ), which combines with BA to form associate compounds of different stochiometries kBA · mBZ (k, m = 0.1,2,….). They proposed that the associate compounds have a synergic effect on the electrodeposition of zinc. In addition, results obtained previously by our group [21] confirm that BA does not form complexes with Zn(II) or Co(II), indicating that its action is principally on the substrate surface.

The influence of BA on the deposition kinetic parameters of each metal was analyzed using the Butler–Volmer equation for the cathodic current of deposition, as proposed by Landolt et al. [6].

Figure 7 shows the plot of potential against $\log|i|$ for the reduction of Zn(II) and Co(II) in the absence of BA. In the potential range −1.23 to −1.43 V vs SCE, the current density of the zinc reduction process is greater than that of the cobalt reduction. This favours preferential deposition of zinc in the alloy and, from a kinetic viewpoint [6, 8], justifies the formation of the anomalous type of codeposit.

When BA is introduced, important changes are observed in the deposition mechanism of the zinc and cobalt metal. In the potential range −1.23 to −1.43 V vs SCE, the current density of cobalt reduction is greater than that of zinc reduction (Figure 8), promoting the deposition of cobalt. Thus, under these conditions,

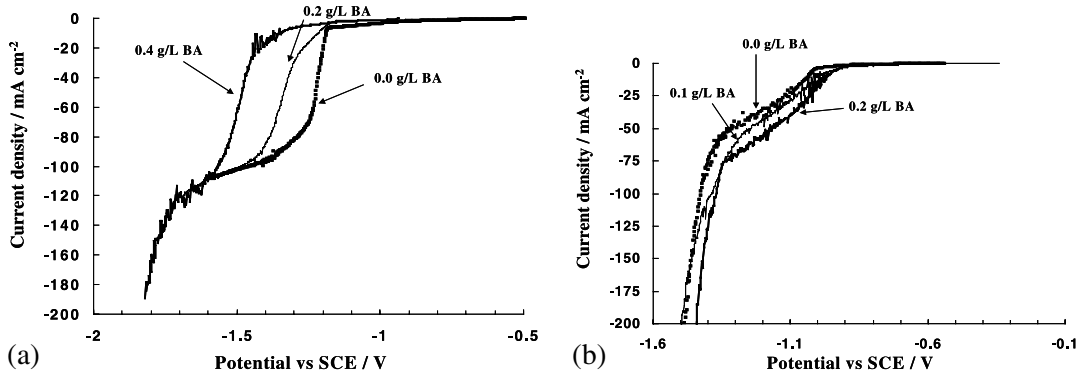

Fig. 6. (a) Linear RDE voltammogram obtained during the reduction of Zn(II) in a solution containing 0.1 M $ZnCl_2$ in 2.8 M KCl + 0.32 M H_3BO_3, at different concentrations of BA. (b) Linear RDE voltammogram obtained during the reduction of Co(II) in a solution containing 0.1 M $CoCl_2.6\,H_2O$ in 2.8 M KCl + 0.32 M H_3BO_3, at different concentrations of BA.

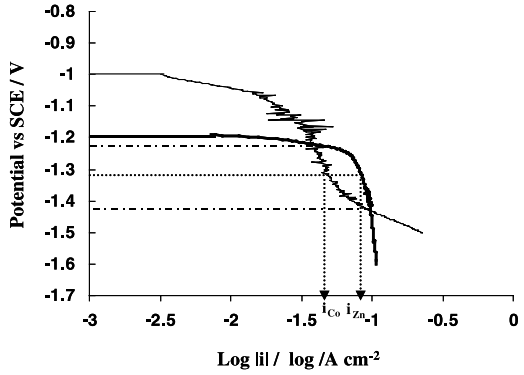

Fig. 7. Tafel plots obtained during the reduction process of: (——) zinc, in a solution containing 0.1 M $ZnCl_2$ in 2.8 M KCl + 0.32 M H_3BO_3, pH 5.0, in the absence of BA, (——) cobalt, in a solution containing 0.1 M $CoCl_2 \cdot 6H_2O$ in 2.8 M KCl + 0.32 M H_3BO_3, pH 5.0, in the absence of BA.

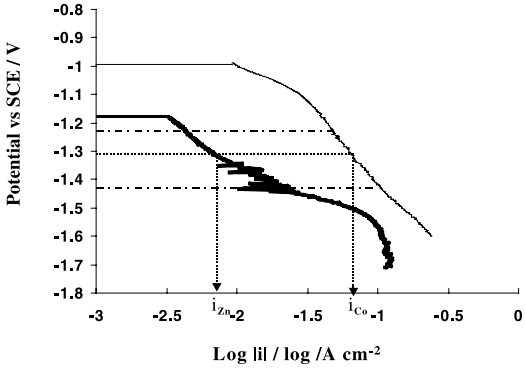

Fig. 8. Tafel plots obtained during the reduction process of: (——) zinc, in a solution containing 0.1 M $ZnCl_2$ in 2.8 M KCl + 0.32 M H_3BO_3, pH 5.0, with 0.2 g L^{-1} BA, (——) cobalt, in a solution containing 0.1 M $CoCl_2 \cdot 6H_2O$ in 2.8 M KCl + 0.32 M H_3BO_3, pH 5.0, with 0.2 g L^{-1} BA.

the Zn–Co alloy forms via a normal type of codeposition [6, 8].

Table 1 lists the values of the exchange current density (i_0) obtained for each metal in the presence of different concentrations of BA. In the absence of BA, $i_{0,Zn}$ is greater than $i_{0,Co}$. In the presence of BA, however, a decrease in $i_{0,Zn}$ and increase in $i_{0,Co}$ were observed with increasing BA concentration. In the concentration range of 0.1 to 0.2 g L^{-1}, the two metals have similar values of exchange current density. From a kinetic viewpoint, this similarity favours the codeposition of both metals. Under these conditions the codeposition mechanism of the Zn–Co alloy is of normal type. At higher concentrations of BA, the value of i_0 of both metals tends to decrease due to the greater importance of the blocking effect of BA on the substrate surface.

Table 1. Variation of $i_{0,Zn}$ and $i_{0,Co}$ as a function of BA concentration

[BA] /g L^{-1}	$i_{0,Zn}$ /mA cm^{-2}	$i_{0,Co}$ /mA cm^{-2}
0.0	30.19	1.09
0.02	2.15	1.29
0.1	2.28	2.31
0.2	1.96	2.36
0.4	1.46	1.09

3.4. *Characterization of coatings*

The Zn–Co alloy electrodeposits were analysed using a range of techniques (SEM, XRD and Auger electron spectroscopy) to determine the influence of BA on the morphology and composition of the deposits. The deposits were potentiostatically grown (−1.35 V vs SCE in the absence of BA, −1.55 V vs SCE in the presence of BA) from base solutions containing a range of BA concentrations until a charge equivalent to a thickness of 6 μm, or 0.65 μm for the Auger electron spectroscopy experiments, was obtained.

3.4.1. *SEM analysis*

Figure 9 shows SEM images of the deposits of Zn–Co alloy obtained from base solutions with and without BA. In the absence of BA, the coatings are made up of tree-like clusters grouped in nodules of diverse dimensions. Furthermore, the formation of interstices between the nodules is also observed (Figure 9(a)). In contrast to the morphology observed in the absence of BA, the deposit that forms in the presence of BA is compact and formed of semi-spherical clusters. No interstices are observed between the clusters, indicating that the coating covers the entire surface (Figure 9(b)). In addition, the size of the clusters decreases with increasing BA concentration (Figure 9(c)), yielding compact shiny deposits at high BA concentrations.

The roughness was evaluated along a representative line of length 3 mm using a profilometer. The parameters R_p (distance from the mean line to the highest peak) and R_t (distance from the highest peak to the deepest valley) were calculated from five measurements. For the deposits obtained in the absence of BA (Figure 9(a)), R_p and R_t were 5.54 μm and 14.15 μm, respectively, while for the deposits obtained in the presence of BA (Figure 9(c)), R_p and R_t were lower (1.09 μm, and 1.77 μm, respectively). These results indicate that BA induces the formation of compact and smooth deposits.

3.4.2. *X-ray diffraction analysis (XRD)*

The XRD pattern shows the formation of lines corresponding to η-phase zinc (101) (Figure 10) and additional lines that can be indexed considering a Zn + Co γ-phase [17]. In addition, an increase is observed in the intensity of the lines of crystalline cobalt (αCo) as the concentration of BA increase from 0.0 to 0.2 g L^{-1}. Beyond this range, intensity decreases for the αCo line, and increase for the γ-phase line.

3.4.3. *Auger spectroscopic analysis*

The concentration profiles of the elements were analysed by Auger electron spectroscopy, sputtering the sample

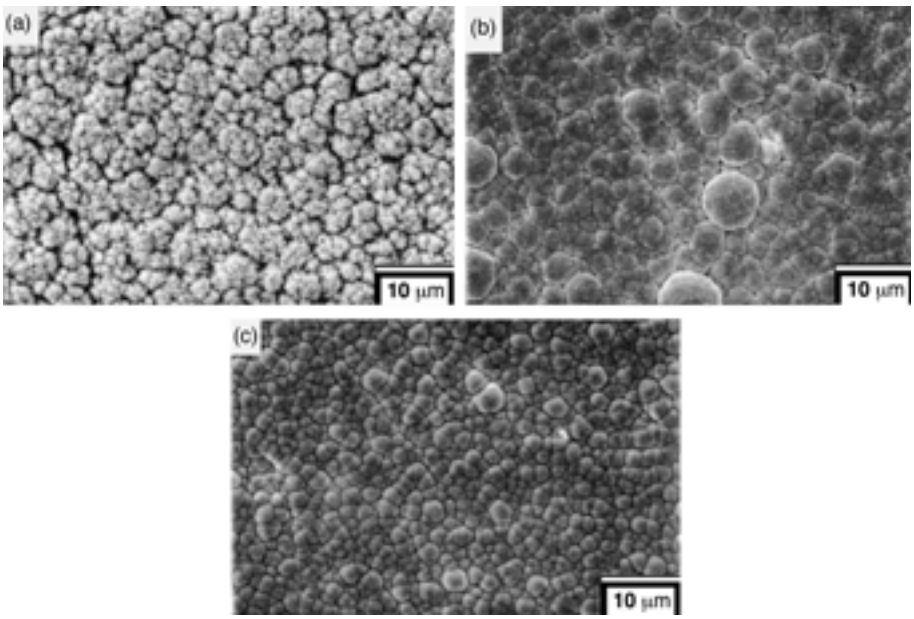

Fig. 9. SEM images of coatings obtained from base solutions with different BA concentrations. (a) 0.0, (b) 0.1 and (c) 0.2 g L^{-1} BA.

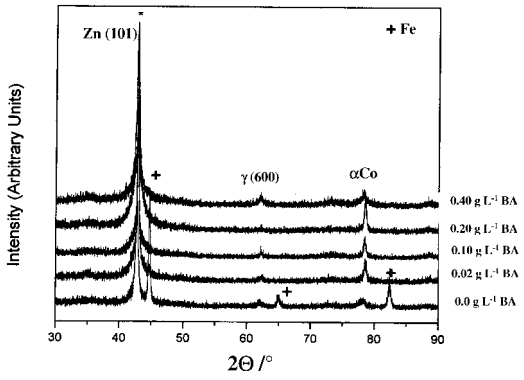

Fig. 10. X-ray diffraction profiles of electrodeposits obtained on 1018 steel substrates from solutions with different BA concentrations.

with Ar^+ ions accelerated to 3 keV. The analysis of the sample was carried out until the substrate was reached.

Figure 11(a) shows the concentration profiles of the elements in the coating formed in the solution without BA. The composition of the coating changes with depth. The lower layers of the coating (i.e., longer sputtering times) contain high concentrations of zinc and oxygen. In contrast, the concentration of cobalt in the lower layers is less than 2% and increases to 3% before remaining constant through the entire thickness of the coating. The presence of oxygen in the lower layers of the coating can be explained in terms of the periodic formation and dissolution of a thin layer of zinc hydroxide ($Zn(OH)_{2(s)}$) produced as a result of the pH increase at the interface. At the surface of the coating (sputtering time < 20 min), a higher concentration of oxygen is present due to surface oxidation.

In the presence of BA (Figure 11(b)), the concentration profile exhibits a significant decline in the amount of oxygen in the lower layers of the coating. Moreover, after removing the layer of zinc oxide from the surface (sputtering time > 20 min), the relative concentration of the elements is constant over the entire coating thickness. In addition, the percentage of cobalt in the

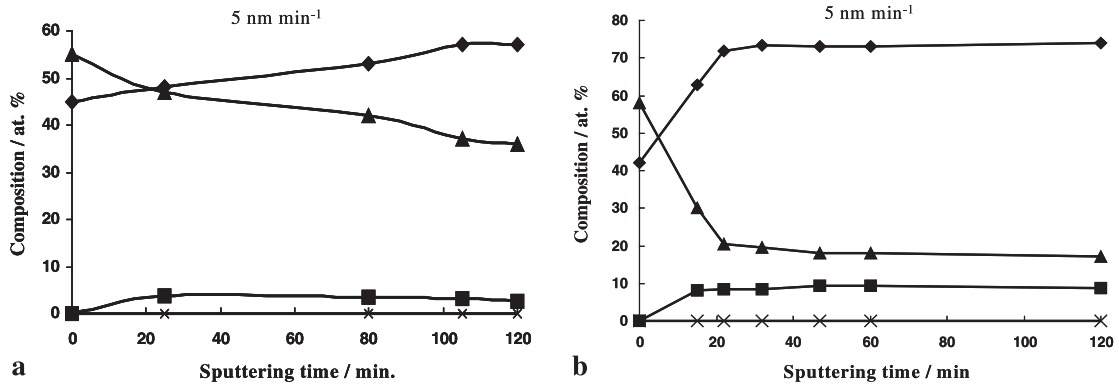

Fig. 11. Auger spectroscopy of concentration profiles distribution of elements (♦) Zn, (■) Co, (▲) oxygen, and (×) iron, in coatings of Zn–Co alloy obtained from base solutions with different BA concentrations: (a) without BA and (b) 0.2 g L^{-1} BA.

coating is greater than that observed obtained in the absence of BA.

4. Conclusions

In the absence of BA, the deposits formed correspond to a Zn–Co alloy rich in zinc. The electrochemical study showed that zinc is deposited preferentially with respect to cobalt, proving that under these conditions the alloy codeposition process is anomalous. This behaviour can be explained by considering the kinetic parameters of the deposition of the metals. The exchange current density for zinc ($i_{0,Zn}$) is greater than that for cobalt ($i_{0,Co}$), indicating that the deposition of zinc is kinetically favoured. Furthermore, analysis of the concentration profiles through the coating, as determined using Auger spectroscopy, revealed the presence of oxygen in the lower layers of the coating. The presence of oxygen can be attributed to the formation of zinc hydroxide on the substrate surface as a result of an increase in pH at the interface.

Addition of BA to the solution caused significant change in the codeposition mechanism. The voltammetric study showed that the preferential deposition of zinc is inhibited in solutions containing BA. In addition, RDE voltammetric analysis of the deposition of each metal showed that BA acts in a selective manner. On the one hand, the presence of BA leads to an increase in the discharge overpotential of zinc without significant modification of its limiting current density ($i_{lim,Zn}$), and BA also induces an increase in the limiting current density of cobalt ($i_{lim,Co}$) without modifying its discharge overpotential. On the other hand, BA causes a decrease in the exchange current density of zinc, $i_{0,Zn}$, and an increase in the exchange current density of cobalt ($i_{0,Co}$). For BA concentrations of 0.1 to 0.2 g L^{-1}, the exchange current densities of Zn and Co are similar, indicating that normal codeposition of the alloy is favoured.

Analysis of the concentration profiles through the coatings by Auger spectroscopy showed that the deposits formed in solutions containing BA are of homogeneous composition, with considerably lower levels of oxygen in the lower layers of the coating. This confirms that the additive BA inhibits the formation of zinc hydroxide on the substrate surface. In addition, the percentage of cobalt in the coatings was higher in coatings deposited from solutions containing BA.

In addition to the modification of the codeposition mechanism of the Zn–Co alloy from anomalous to normal, SEM analysis of the coating morphologies showed that smaller clusters form in the presence of BA, promoting the formation of compact, shiny coatings.

Acknowledgement

The authors are grateful for financial assistance provided by CONACyT (Consejo Nacional de Ciencia y Tecnología, México, proyecto 31411-U and PCP 000/04).

References

1. A. Brenner, 'Electrodeposition of Alloys' Vols. 1 and 2 (Academic Press. New York/London, 1963).
2. K. Higashi, H. Fikushima, T. Urokawa, T. Adaniya and K. Matzudo, *J. Electrochem. Soc.* **128** (1981) 2081.
3. M.I. Nicol and H.I. Philip, *J. Electroanal. Chem.* **70** (1976) 233.
4. H. Yan, J. Downes, P.J. Boden and S.J. Harris, *J. Electrochem. Soc.* **143** (1996) 1577.
5. R. Fratesi and G. Roventi, *J. Appl. Electrochem.* **22** (1992) 657.
6. D. Landolt, *Electrochim. Acta* **39** (1994) 1075.
7. M.F. Mathias and T.W. Chapman, *J. Electrochem. Soc.* **134** (1987) 1408.
8. Z. Panossian, *Metal Finish.* June (1999) 88.
9. R. Fratesi, G. Roventi, G. Giluliani and C.R. Tomachuk, *J. Appl. Electrochem.* **27** (1997) 1088.
10. M. Yunus, C. Capel-Boute and C. Decroly, *Electrochim. Acta* **10** (1965) 885.
11. E. Gómez and E. Vallés, *J. Electroanal. Chem.* **397** (1995) 177.
12. E. Gómez, E. Vallés, P. Gorostiza, J. Servat and F. Sanz, *J. Electroanal. Chem.* **142** (1995) 4091.
13. M.L. Alcalá, E. Gómez and E. Vallés, *J. Electroanal. Chem.* **370** (1994) 73.
14. E. Gómez and E. Vallés, *J. Electroanal. Chem.* **421** (1997) 157.
15. H.M. Wang and T.J. O'Keefe, *J. Appl. Electrochem.* **24** (1994) 900.
16. V.D. Jovic, R.M. Zejnilovic, A.R. Despic and J.S. Stevanovic, *J. Appl. Electrochem.* **18** (1998) 511.
17. E. Gómez, X. Alcobe and E. Vallés, *J. Electroanal. Chem.* **505** (2001) 54.
18. D. Mockute and G. Bernotiene, *J. Appl. Electrochem.* **27** (1997) 691.
19. A. Stankeviciute, K. Leinartas, G. Bikulcius, D. Virbalyte, A. Sudavicius and E. Juzeliunas, *J. Appl. Electrochem.* **28** (1998) 89.
20. H. Dasm and I.M. Croll, *J. Electrochem. Soc.* **112** (1965) 771.
21. G. Trejo, R. Ortega B and Y. Meas, *in* Proceedings of the XIV Congreso Sociedad Mexicana de Electroquímica, Mayo (2001).